



HAL
open science

Sequestration of Proteins in Stress Granules Relies on the In-Cell but Not the In Vitro Folding Stability

Nirnay Samanta, Sara Ribeiro, Mailin Becker, Emeline Laborie, Roland Pollak, Stepan Timr, Fabio Sterpone, Simon Ebbinghaus

► To cite this version:

Nirnay Samanta, Sara Ribeiro, Mailin Becker, Emeline Laborie, Roland Pollak, et al.. Sequestration of Proteins in Stress Granules Relies on the In-Cell but Not the In Vitro Folding Stability. *Journal of the American Chemical Society*, 2021, 143 (47), pp.19909-19918. 10.1021/jacs.1c09589 . hal-03827043

HAL Id: hal-03827043

<https://hal.science/hal-03827043>

Submitted on 24 Oct 2022

HAL is a multi-disciplinary open access archive for the deposit and dissemination of scientific research documents, whether they are published or not. The documents may come from teaching and research institutions in France or abroad, or from public or private research centers.

L'archive ouverte pluridisciplinaire **HAL**, est destinée au dépôt et à la diffusion de documents scientifiques de niveau recherche, publiés ou non, émanant des établissements d'enseignement et de recherche français ou étrangers, des laboratoires publics ou privés.

Sequestration of Proteins in Stress Granules Relies on the In-Cell but Not the *In Vitro* Folding Stability

Nirnay Samanta,^{||} Sara S. Ribeiro,^{||} Mailin Becker, Emeline Laborie, Roland Pollak, Stepan Timr,^{*} Fabio Sterpone,^{*} and Simon Ebbinghaus^{*}



Cite This: *J. Am. Chem. Soc.* 2021, 143, 19909–19918



Read Online

ACCESS |



Metrics & More

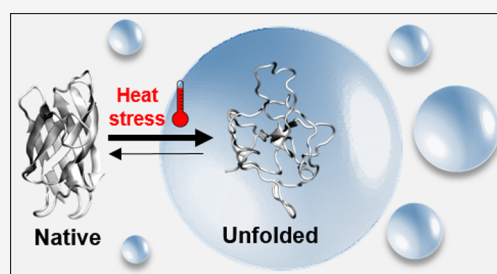


Article Recommendations



Supporting Information

ABSTRACT: Stress granules (SGs) are among the most studied membraneless organelles that form upon heat stress (HS) to sequester unfolded, misfolded, or aggregated protein, supporting protein quality control (PQC) clearance. The folding states that are primarily associated with SGs, as well as the function of the phase separated environment in adjusting the energy landscapes, remain unknown. Here, we investigate the association of superoxide dismutase 1 (SOD1) proteins with different folding stabilities and aggregation propensities with condensates in cells, *in vitro* and by simulation. We find that irrespective of aggregation the folding stability determines the association of SOD1 with SGs in cells. *In vitro* and *in silico* experiments however suggest that the increased flexibility of the unfolded state constitutes only a minor driving force to associate with the dynamic biomolecular network of the condensate. Specific protein–protein interactions in the cytoplasm in comparison to SGs determine the partitioning of folding states between the respective phases during HS.



INTRODUCTION

The intracellular liquid–liquid phase separation (LLPS) of proteins and RNA leading to the formation of membraneless organelles (MLOs) is now established as a fundamental process in cell biology, exhibiting functions in cellular signaling,^{1,2} transcriptional³ and translational⁴ regulation, enzymatic activity,⁵ and stress response.^{6,7} In fact, MLOs formed during stress conditions are part of a more complex orchestrated cellular feedback that also encompasses the formation of reversible protein aggregates and filaments, all serving to increase fitness and survival.^{6,8,9} Stress granules (SGs) are one of such type of cytoprotective assemblies, formed in response to heat stress (HS), that among under functions are known to recruit and transiently store misfolded proteins.^{6,10–13}

HS leads to local or global unfolding of proteins, resulting in the exposure of hydrophobic segments that were otherwise buried in native conditions.¹⁴ The protein quality control (PQC) machinery (chaperones, ubiquitin-proteasome, or autophagy), engages with such unfolded/misfolded states, refolding, shielding, or degrading them, thus precluding toxic aggregation.^{12,15–17} These actions are usually rationalized with partition models, where clients can directly bind to PQC as monomers, oligomers, or aggregates, with all these states being further sequestered by SGs and thus optimizing client clearance.^{6,11,17–21} Nevertheless, mutations or failure in the PQC promoted by cellular stress or aging leads to deleterious changes in the material properties of the SG components, triggering pathological phase transitions.^{18,22–24}

The formation of SGs involves homotypic as well as heterotypic multivalent interactions among proteins with folded and intrinsically disordered regions (IDPRs) and RNA.²⁵ Simplistic approaches developed to reconstitute *in vitro* SGs have shown that homotypic interactions within their single components such as Fused in Sarcoma (FUS),^{22,26} ribonucleoprotein A1 (hnRNPA1),²⁷ Ras GTPase-activating protein-binding protein (G3BP),²⁸ or RNA binding protein TDP-43²⁹ are sufficient to induce LLPS. While lower multivalence and structural rigidity of globular proteins are thought to inherently reduce the propensity for LLPS,³⁰ their unfolded forms were recently shown to drive aggregation-mediated phase separation via homotypic interactions.³¹ Nevertheless, it remains unknown if unfolded states constitute an omnipotent driving force when considering heterotypic interactions in functional condensates^{32,33} such as SGs. This is important as homotypic-driven aberrant phase transitions are bypassed inside MLOs by “heterotypic buffering”, which refers to the ability of heterotypic interactions to suppress the excess of homotypic interactions within the condensates.³⁴ Considering the intrinsic stickiness of unfolded states and their well-known tendency to form (toxic) aggregates,³⁵ it is crucial to

Received: September 9, 2021

Published: November 17, 2021



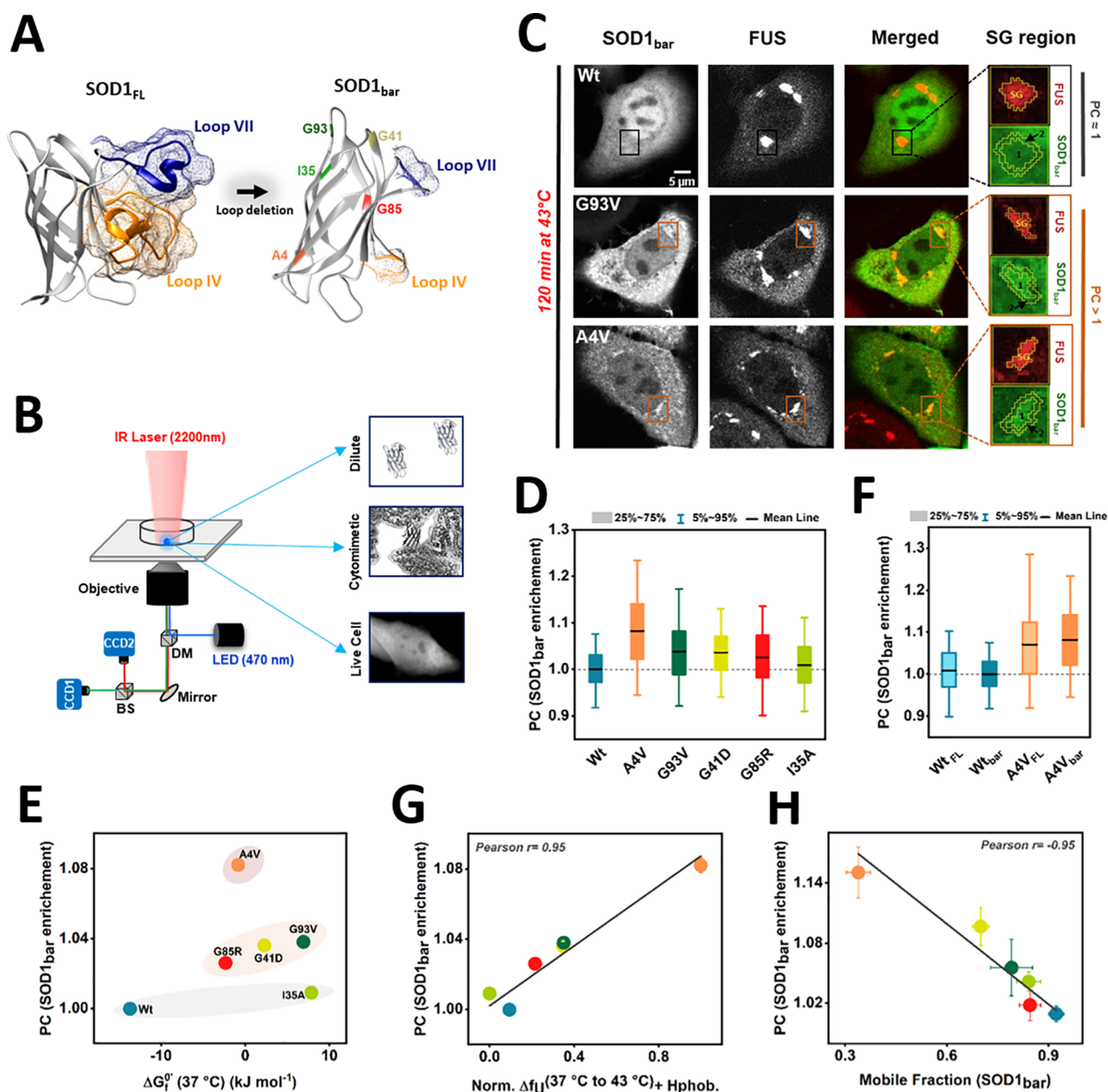


Figure 1. SOD1_{bar} as a sensor to measure protein unfolding and SG association in-cell and *in vitro*. (A) SOD1_{FL} (Protein Data Bank (PDB) ID: IHL5) and SOD1_{bar} (PDB ID: 4BCZ), with mutations A4V, I35A, G41D, G85R, and G93V highlighted. Images were assembled using UCSF Chimera.⁵² (B) Schematic representation of the FReI technique with two cameras (CCD1 and CCD2). DM and BS represent dichroic mirror and beam splitter, respectively. (C) Exemplary images of HeLa^{FUS-mCh} cells showing different partitioning of the SOD1_{bar}-AcGFP1 mutants G93V and A4V. Enrichment of SOD1_{bar}-AcGFP1 was defined by a local apparent partition coefficient (PC) > 1, determined as the ratio of the mean fluorescence intensity inside the SG (region 1) and the mean fluorescence intensity at 0.6 μm (region 2) from the SG (right zoom-in). (D) PC of SOD1_{bar} after 120 min at 43 °C (*N* = 437 to 523 SGs). PCs of mutants A4V, G93V, G41D, and G85R are significantly higher than Wt. (E) PCs as a function of ΔG_f^o at 37 °C. The values are significantly different between each of the three defined clusters: Wt and I35A (light gray), G93V, G41D, and G85R (light brown) and A4V (light red). (F) PCs of SOD1_{bar}-Wt and SOD1_{FL}-Wt and the respective A4V mutants. No statistical significance is found between the PCs of SOD1_{bar} and SOD1_{FL} for both Wt and A4V. (G) Correlation between SOD1_{bar} PCs and the scaled sum [norm. Δf_U^{37-43°C} + norm. Hphob]. We normalized Δf_U^{37-43°C} values for the different constructs (1 represents the highest Δf_U^{37-43°C}, while 0 represents the lowest one). Similarly, Hphob was normalized from 1 (highest) to the 0 (lowest) within the different SOD1_{bar} sequences. Finally, we sum up the normalized values, [norm. Δf_U^{37-43°C} + norm. Hphob] and scaled between 0 and 1 (lowest to highest). (H) Correlation between mobile fractions (MFs) inside SGs and PCs. The statistical analyses reported in panels D–F were carried out using one-way ANOVA, followed by a post hoc Tukey test for multiple comparisons, computed with a confidence interval of 95%. The values in panels E, G, and H are presented as mean ± SEM.

investigate how these states engage in the condensate network and how they modify homotypic/heterotypic contacts preserving functional as opposed to pathological phase transitions.

In this study, we investigate the function of LLPS as a cytoprotective mechanism, sequestering unfolded, misfolded, or aggregated protein under cellular stress condition. Considering the in-cell folding and aggregation landscape of

superoxide dismutase 1 (SOD1),^{36–39} involved in the disease progression of amyotrophic lateral sclerosis (ALS),⁴⁰ we identify the folding states that are sequestered by SGs. In this context, we test the hypothesis if the protein unfolding process constitutes an omnipotent driving force for the association with condensates.

RESULTS AND DISCUSSION

The Load of Unfolded Protein and Its Effect on Condensate Association under HS in HeLa Cells and *In Vitro*. ALS-related full-length (SOD1_{FL}) mutants were previously shown to accumulate and aggregate inside SGs;^{18,41,42} however, the folding states that associate with these condensates remain unknown. To investigate the role of unfolded SOD1 in SG association independently of aggregation, we study SOD1_{bar} in reference to SOD1_{FL}. SOD1_{bar} is a monomeric β -barrel protein, where loops IV and VII from SOD1_{FL} were swapped by Gly-Ala-Gly linkers, leading to breakage of the dimer interface, catalytic inactivation and higher thermodynamic stability⁴³ (Figure 1A). Importantly, removal of Zn²⁺ and Cu²⁺ coordination sites as well as replacement of Cys-6 and Cys-111,146 by Ala and Ser diminishes the metal-loss-induced misfolding⁴⁴ and the in-cell aggregation propensities at both physiological⁴⁵ and HS conditions (Figure S1). On the basis of our prior knowledge of the in-cell modified standard state folding free energies at 37 °C ($\Delta G_f^{\circ'}$),³⁹ we examined the SG association of a set of specifically destabilized SOD1_{bar} mutants (G85R, A4V, G41D, G93V, and I35A) (Figure 1A). The choice of mutants with distinct $\Delta G_f^{\circ'}$, combined with fast and reversible 2-state folding and lack of aggregation (except A4V, Figure S2),³⁹ allowed us to vary the amount of unfolded protein upon HS in the respective experiments. Stability measurements to determine T_m and $\Delta G_f^{\circ'}$ under different conditions were conducted by Fast Relaxation Imaging (FReI)⁴⁶ (Figure 1B and S3); aggregation and SG association were monitored by temperature-controlled confocal laser scanning techniques (see the Supporting Information, “Materials and Methods” section).

Sequestration of SOD1 in SGs under HS Conditions. We first investigated if partitioning of SOD1_{bar} into SGs depends on the in-cell $\Delta G_f^{\circ'}$. HeLa^{FUS-mCh} cells coexpressing AcGFP1-SOD1_{bar}-Wt and mutants were exposed to HS at 43 °C for 120 min following a previously established protocol.¹⁸ We quantified the partitioning of SOD1_{bar} by determining the local apparent partition coefficient (PC) as the ratio between the mean fluorescence intensity inside SGs ($FI_{\text{mean}}^{\text{SG}}$) and the mean fluorescence intensity in the immediate surroundings ($FI_{\text{mean}}^{\text{out}}$) using confocal microscopy. Exemplary images and corresponding PCs of SOD1_{bar}-Wt and mutants G93V and A4V are depicted in Figure 1C. PC values of >1 are specific indicators of SOD1_{bar} accumulation inside SGs, as defined previously by colocalization analysis carried out for SOD1_{FL} and FUS or G3BP1.¹⁸ Importantly, PCs are concentration-independent as long as binding-site occupancy does not reach its maximum.⁴⁷ Indeed, plotting PCs against the different SOD1_{bar} expression levels (based on the average fluorescence intensity in the cytoplasm) for each construct shows no dependency on the intracellular concentrations (Figure S4), suggesting that such levels are below saturation.

We observed a significant increase in the PCs for SOD1_{bar} mutants (A4V, G93V, G41D, and G85R) in comparison to the Wt protein, while no difference was found for I35A (Figure 1D). We further plotted PC values as a function of $\Delta G_f^{\circ'}$ at 37

°C for each construct and classified them into three clusters, with each cluster containing PC values which are statistically not distinguishable between them (Figure 1E). Both the most and least stable constructs (Wt and I35A) display no preferential partitioning inside SGs, while constructs of intermediate stabilities (G93V, G41D, and G85R) lead to SOD1_{bar} enrichment, being distinctively high for A4V. This mutational effect is consistent with earlier reports of the accumulation of the corresponding SOD1_{FL} mutants inside SGs,^{18,41,42} suggesting that the destabilization of the β -barrel structure may constitute the main driving force for SGs accumulation. We further verified this conclusion by comparing the PCs of SOD1_{bar}-Wt and SOD1_{bar}-A4V with the more aggregation-prone SOD1_{FL}-Wt and SOD1_{FL}-A4V.⁴⁵ As expected, we found no significant change between SOD1_{bar} and SOD1_{FL} PCs for both Wt and A4V (Figure 1F), while this same construct (SOD1_{FL}-A4V) shows higher aggregation in the cytoplasm when compared to its barrel counterpart (Figure S1). Comparable levels of aggregation were found for all SOD1_{bar} mutations (Figure S2), except A4V, suggesting that SGs-mediated sequestration is independent of the intracellular aggregation propensity of the protein during HS.

We next explored the idea that the extra load of unfolded protein upon HS¹⁴ could reinforce partitioning of SOD1_{bar} mutants into SGs, as pre-existing unfolded proteins remain bound to PQC^{17,48} and are thus unavailable to be recruited. We determined the unfolded fractions for each construct at 37 and 43 °C from $\Delta G_f^{\circ'}$ at these same temperatures and plotted the change, $\Delta f_U^{37-43^\circ\text{C}}$ against the different PCs (Figure S5A). We found no apparent correlation (Pearson $r = 0.74$) indicating that HS induced unfolding is not the only requisite for SG association. We then tested if accounting for the increase in hydrophobicity upon unfolding increases this correlation, as previous studies suggested that recruitment of mutant SOD1_{FL} into SGs was mediated by hydrophobic interactions.⁴¹ We analyzed if mutations resulting in increased hydrophobicity could promote partitioning of HS-induced unfolded SOD1_{bar} in SGs. As such, we first computed the hydrophobicity (Hphob) based on solvent accessible surface areas (SASAs) and overall transfer free energies from water to cyclohexane resulting from adding up the individual values obtained for each residue in the unfolded SOD1_{bar} (Table S1, see the Supporting Information, “Materials and Methods” section). To consider the hydrophobicity change Figure S5B upon unfolding in the $\Delta f_U^{37 \text{ to } 43^\circ\text{C}}$ (no correlation of PCs was found with the hydrophobicity alone, Figure S5B), we plotted the scaled sum [norm. $\Delta f_U^{37-43^\circ\text{C}}$ + norm. Hphob.] (1 to 0, highest to lowest), following the strategy proposed previously.^{49,50} We found a significant positive correlation with the PCs (Pearson $r = 0.95$, Figure 1G). We also plotted PCs as a function of $\Delta f_U^{37-43^\circ\text{C}}$ and Hphob in a 3D plot (see Figure S5C). Both the approaches suggest that the increased amount of unfolded protein by HS, paired with an increase in hydrophobicity of the unfolded state, contributes to SOD1_{bar} partitioning into SGs. Specifically, this effect likely relies on interactions of hydrophobic residues accessible in unfolded SOD1_{bar}. This interpretation would be in line with prior assignments of homotypic intermolecular hydrophobic contacts as determinants for LLPS of unfolded barnase³¹ and elastin.⁵¹

Finally, we investigated diffusion properties of SOD1_{bar} in SGs to probe for a reduced mobility of the protein in comparison to the cytoplasm, suggesting stronger interactions

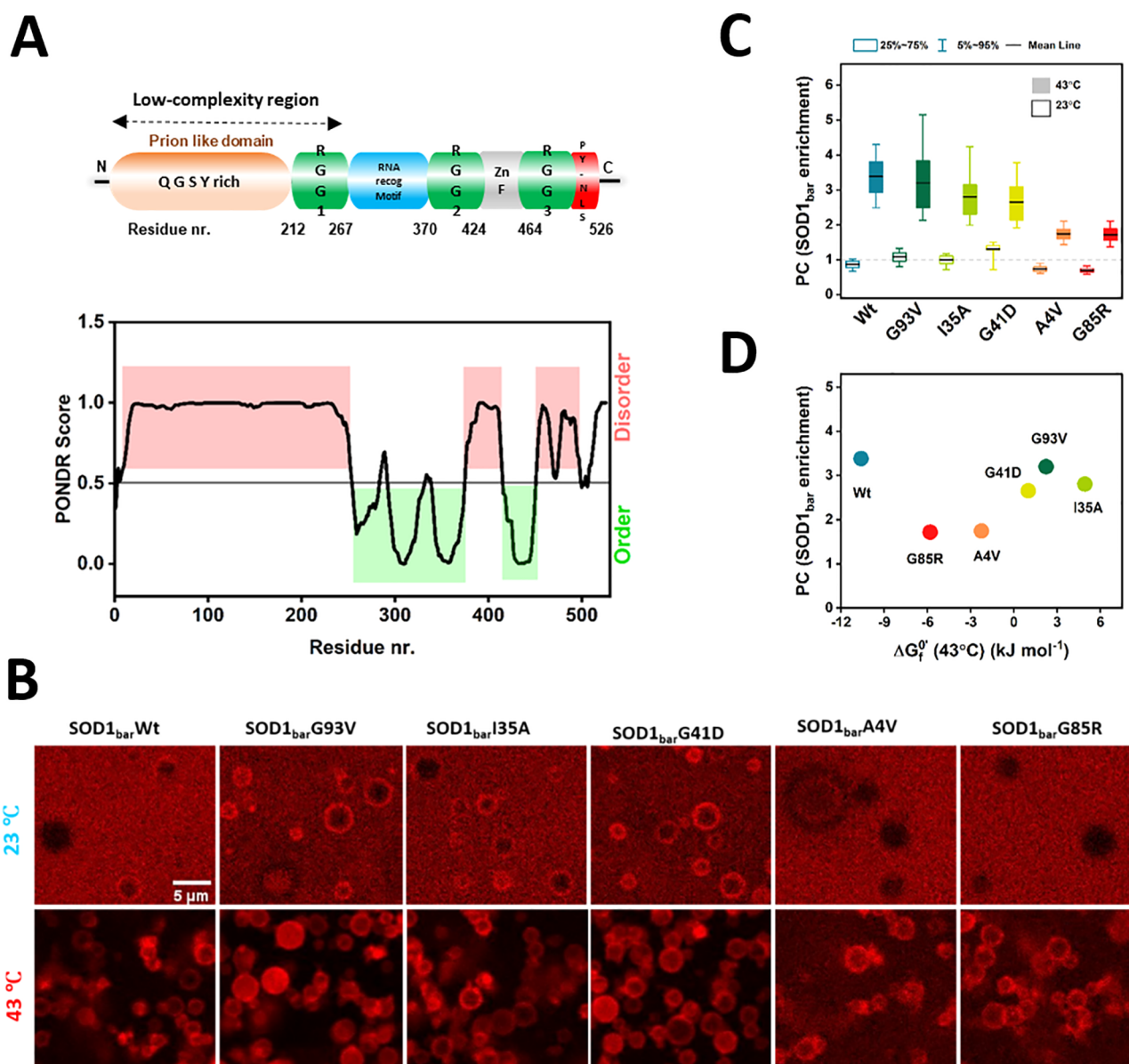


Figure 2. Association of SOD1_{bar} with FUS droplets *in vitro*. (A) Schematic representation of the different FUS domains with predicted (dis)ordered domains by Prediction of Natural Disorder Regions (PONDNR) Score bioinformatics tool.⁵⁶ (B) Exemplary images (mCherry channel) of SOD1_{bar} added to FUS droplets (in buffer, pH 7.5) after 60 min of incubation at 23 or 43 °C. (C) PCs after 60 min of incubation shown as whisker box plots ($N = 41–203$ droplets for 23 °C, $N = 422–895$ droplets for 43 °C). The values are significantly different (except G85R vs A4V) among each other. Significant tests were carried out by one-way ANOVA analysis, followed by post hoc Tukey test for multiple comparisons, computed with a confidence interval of 95%. (D) Mean values of PCs (at 43 °C) plotted against ΔG_i^0 at 43 °C.

and association.¹⁸ We therefore carried out fluorescence recovery after photo bleaching (FRAP) experiments in SGs and in the cytosol (Figure S6A). In the SG environment, we found lower mobile fractions for A4V and G41D mutations when compared to the Wt and higher cytosolic mobility of A4V in contrast to that associated with the condensates (Figure S6B), suggestive of stronger interactions in SGs versus the cytoplasm. Consistently, we observed a significant negative correlation between the PCs and MFs of all SOD1_{bar} proteins, with larger partitioning of mutant SOD1_{bar} leading to lower mobility and thus stronger association with SGs (Figure 1H).

In summary, ALS-linked mutants of SOD1_{bar}, as well as their SOD1_{FL} counterparts associated with SGs under HS conditions, suggesting that such partitioning is independent of metal binding, dimerization sites, and aggregation

propensity. The sequestration of proteins in SGs rather relies on the in-cell folding stability suggesting that conformers belonging to the unfolded state ensemble participate in the homotypic and heterotypic protein–protein interactions that compose these cytoprotective assemblies.

SOD1_{bar} Partitioning into FUS Droplets *In Vitro* under HS Conditions. We next investigate the sequestration of unfolded SOD1 proteins in a cell-free environment by using a simplistic three-component system encompassing FUS condensates and SOD1 protein in dilute solution. The rationale is to probe if SOD1_{bar} condensate association observed in the cell can be solely attributed to protein unfolding as a driving force. We followed a pre-established protocol to purify (see the Supporting Information, “Materials and Methods” section, Figure S7) and induce droplet formation of full-length FUS

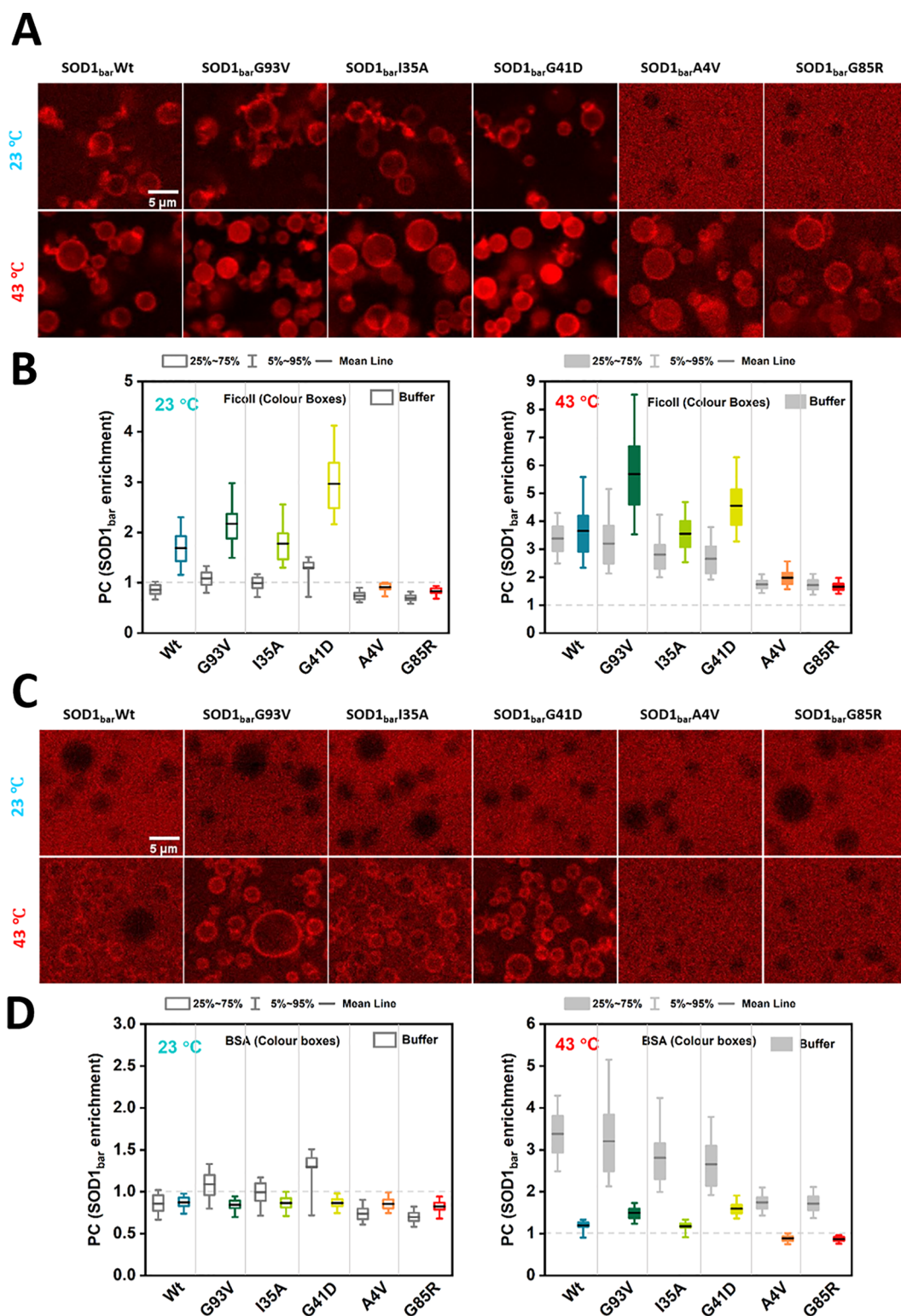


Figure 3. Effect of crowding (*in vitro*) on SOD1_{bar} association with FUS droplets at different temperatures. Exemplary images (mCherry channel) of SOD1_{bar} enrichment/depletion in the presence of (A) 15% (*w/v*) Ficoll 70 and (C) 20% (*w/v*) BSA, after 60 min of incubation at 23 and 43 °C. (B and D) PCs measured after 60 min at 23 and 43 °C in the presence of Ficoll and BSA. PCs in buffer (data from Figure 2) are shown as gray box plots for comparison. (*N* = 96–304 droplets for 23 °C, *N* = 263–706 droplets for 43 °C). The values are significantly different among each other [except for (B) G85R (in buffer) vs G85R (in Ficoll), Wt (in Ficoll) vs I35A (in Ficoll), and (D) Wt (in BSA) vs I35A (in BSA)]. Significance tests were carried out by one-way ANOVA analysis, followed by post hoc Tukey test for multiple comparisons, computed with a confidence interval of 95%.

(Figure 2A),^{18,22,26,53–55} together with SOD1_{bar}. We studied the association of SOD1_{bar} with FUS droplets before and after

the HS, using confocal microscopy, where the transmitted signal (for the bright field image, Figure S8A) allowed the

Table 1. Interaction Energies of 10 SOD1_{bar} with BSA and FUS LCD in the Two Solutions^a

	FUS LCD–SOD1 _{bar} (f)	BSA–SOD1 _{bar} (f)	FUS LCD–SOD1 _{bar} (u)	BSA–SOD1 _{bar} (u)
energy [kJ mol ⁻¹]	-35.2 ± 1.7	-41.4 ± 6.3	-29.3 ± 2.5	-46.8 ± 1.7

^aSolutions were obtained at 27 °C and considering the folded (f) and unfolded (u) SOD1_{bar}. Error bars were estimated via block analysis. The 100 g/L BSA concentration was used in this comparison, and the SOD1_{bar} unfolded state was modeled as a floppy elastic network (see the “Materials and Methods” section in the Supporting Information). The observed trends are also maintained at a higher temperature; see Figure S13C.

detection of FUS condensates and mCherry fluorescence emission was used to identify SOD1_{bar}. While at 23 °C the FUS droplets were either visually depleted or enriched in the peripheral region with SOD1_{bar}-Wt and mutants, at the HS temperature (43 °C) we found a significant enhancement of SOD1_{bar} accumulation for all the constructs (Figure 2B). We further determined the PC ($Fl_{\text{mean}}^{\text{Droplet}}/Fl_{\text{mean}}^{\text{outDroplets}}$) of SOD1_{bar} to quantify its enrichment in the FUS compartments at the HS condition. Similar to the in-cell measurements, where partitioning of SOD1 inside SGs reaches a steady-state condition after 120 min,¹⁸ we conducted HS over 60 min, until such equilibrium conditions were equally attained (Figure S9). As depicted in Figure 2C, the PC values for all the SOD1_{bar} constructs increase after HS to values of >1, suggesting a general preferential partitioning into FUS condensates. This HS induced SOD1_{bar} partitioning is corroborating the observed SG sequestration in cells. In contrast, the PC values do not show a correlation between ΔG_f° of the SOD1_{bar} and condensate association, as SOD1_{bar}-Wt showed higher PCs than all mutants (Figure 2D). Thus, the *in vitro* experiments suggest that unfolding of SOD1_{bar} and the acquired flexibility and hydrophobicity of the unfolded state, may not constitute the main driving force for condensate association upon HS.

The results rather suggest that a delicate balance of protein–protein interactions in the two phases governs the partitioning. The SOD1_{bar} point mutations appear to be decisive in changing this balance, in line with our previous studies showing that the stability of SOD1_{bar} in the cell compared to *in vitro* changes significantly with specific point mutations.³⁹ Correspondingly, we here observed that single-point mutations can even lead to the formation of multiphase condensates.^{57,58} While we found that SOD1_{bar}-G93V and SOD1_{bar}-G41D accumulate homogeneously in the droplets, SOD1_{bar}-Wt, SOD1_{bar}-A4V, and SOD1_{bar}-G85R accumulate predominantly in the periphery regions (Figure S8B).

Changes in protein–protein interactions may also be due to altered FUS–FUS interactions upon heat shock.⁵⁹ Indeed, we found that FUS droplets in the absence and presence of SOD1_{bar} show a noticeably modified size and morphology (see Figure S8A and S10) after HS, indicative that the HS condition modifies the FUS–FUS interactions as well as the FUS–SOD1_{bar} network.^{60,61} We speculate that part of this change may be attributed to the unfolding of the RBD of FUS (residue numbers 285–371, Figure 2A), exposing additional residues accessible for preferential interactions with SOD1_{bar}.^{62,63}

In summary, the HS conditions enhance SOD1_{bar} partitioning into FUS condensates depending on single-point mutations, but in contrast to in-cell experiments, independent of folding stability.

SOD1_{bar} Partitioning in Crowded Solutions. The *in vitro* experiments suggest that the protein–protein interactions that govern partitioning of SOD1_{bar} are sensitive to environmental changes. This may be of particular relevance in cellular health and disease conditions.^{64,65} Concerning effects in the crowded cell arising from volume-exclusion, quinary inter-

actions, or chaperone engagement, it is evident that these factors can modulate both the folding equilibrium^{17,39,66–71} as well as phase separation.^{18,72–75} We deciphered those in cytomimetic media by using Ficoll 70 (15% w/v), known to exert stabilizing excluded-volume effects⁷⁶ ($\Delta\Delta G_f^{\circ}(37\text{ °C}) < 0$), and BSA (20% w/v), known to mimic destabilizing quinary interactions^{39,76} ($\Delta\Delta G_f^{\circ}(37\text{ °C}) > 0$) (Figure S11). We therefore investigated whether these cosolutes that are known to change ΔG_f° have an influence on SOD1_{bar} association with FUS condensates. As depicted in Figure 3A,B, Ficoll 70 solution significantly promotes the SOD1_{bar} partitioning to the FUS condensates, both at 23 and 43 °C, when compared to dilute solution. In contrast, in BSA solution, we observed a considerable decrease of the PCs for SOD1_{bar} even after 60 min of HS (Figure 3C,D).

Both observations suggest that shifting the folding equilibrium toward the folded or unfolded states does not determine SOD1_{bar} partitioning (Figure S12). The results can be rather attributed to the cosolute effects on the LLPS^{74,77,78} driving the separation of both proteins in the system, FUS and SOD1_{bar}. Thereby, Ficoll 70 induced phase separation can be explained by increased depletion attraction^{72,75,77} arising from its exclusion from the FUS–SOD1_{bar} condensate. Likewise, BSA suppresses phase separation presumably by protein–protein interactions weakening the condensate.^{74,77} In fact, BSA was previously shown to suppress phase separation of FUS IDR (amino acids 1–237) due to favorable interactions with FUS,⁷⁵ whose interpretation with the mass action model⁷⁹ suggests few free binding sites in the FUS droplet network, impeding the accommodation of SOD1_{bar}. In other words, BSA colocalizes in FUS droplets as FUS–BSA interactions compete with FUS–SOD1_{bar} association and thus suppress SOD1_{bar} partitioning into the condensates. Alternatively, SOD1_{bar} preferentially binds to BSA in the dilute phase and thus reduces its availability to interact in the FUS droplet phase.

Remarkably, the PCs in BSA are similar to those measured in cellular SGs (Figure 1D), suggesting that BSA acts as a good cytomimetic cosolute for LLPS, in accordance with our previous studies on SOD1_{bar} folding stability.³⁹ Overall, tweaking the folding equilibrium does not modulate SOD1_{bar} association in FUS condensates accordingly, but rather it changes the protein–protein interactions in the respective phases to determine SOD1_{bar} partitioning.

Lattice Boltzmann Molecular Dynamics (LBMD) Simulation to Investigate Interactions of SOD1_{bar} with FUS Low-Complexity Domain (LCD) and BSA. To quantify how the energetics of SOD1_{bar} partitioning into a condensate depends on the folding state of the barrel, we carried out coarse-grained LBMD simulations^{80,81} of folded and unfolded SOD1_{bar} molecules embedded in a high-concentration FUS solution composed of 70 chains of the FUS LCD, mimicking a droplet solution concentration of 150 g/L (Figure S13A). Evaluation of the SOD1_{bar}–FUS LCD interaction energies showed that from the enthalpic point of view the unfolded state of SOD1_{bar} does not interact more

favorably with the FUS LCD domain in comparison to the folded form, with the energy difference for one SOD1_{bar} protein being less than 1 kJ mol⁻¹ (Table 1). In fact, unfolding leads to a change in the specific contacts between SOD1_{bar} and FUS LCD (Figure S13E,F), disfavoring the association of both proteins. These findings agree with the experimental *in vitro* results showing that partitioning of SOD1_{bar} is independent of its folding stability.

A comparison with the interaction energies of SOD1_{bar} embedded in BSA solutions (Table 1) yielded similar results for folded SOD1_{bar} in BSA (100 g/L) (Figure S13B) as in FUS (150 g/L), with SOD1_{bar} experiencing numerous favorable charge–charge contacts in BSA (Figure S13G,H). Moreover, a slight preference for BSA arises when SOD1_{bar} unfolds. However, the magnitude of these interaction differences is very small, on the order of a few kJ mol⁻¹ (Table 1). The comparable energetics in BSA and FUS that we quantified in the simulations rationalizes the suppressing effect of BSA on the SOD1_{bar} partitioning into the FUS phase by proposing that SOD1_{bar}–BSA interactions are at least as favorable as SOD1_{bar}–FUS LCD interactions. Finally, we observed a strong dependence of the SOD1_{bar}–BSA interaction on the concentration of the BSA solution, with the interaction energies increasing more than by a factor of 5 at 300 g/L (see Figure S13D). This points to the delicate role of local protein concentration inside and outside the condensate in determining the partitioning. Estimating the density distribution of proteins across the two-phase boundary is a current challenge and might help to rationalize the differences observed between in-cell and *in vitro* experiments.

CONCLUSION

In this study, we showed that destabilized SOD1_{bar} mutants, independent of the aggregation processes, associate with SGs under HS conditions, suggesting that the unfolded states engage in the homotypic and heterotypic interactions that drive their formation. *In vitro* studies in the reconstituted FUS environment, however, revealed that the intrinsic flexibility of the SOD1_{bar} unfolded state, despite altering the protein's interactions with the condensate, does not constitute an omnipotent driving force for condensate association. Studies in cytomimetic media paired with LBMD simulations suggest that specific protein–protein interactions, subject to single-point mutations, determine the partitioning between the two phases. Further investigations in this direction will require the inclusion of different interaction partners of SOD1 in the SG environment using *in vitro* reconstitutions with other well-known condensate components, such as G3BP1,⁴¹ or PQC components such as chaperones.¹⁸ In fact, the small but significant changes in the in-cell PC values of the SOD1_{bar/FL} mutants in comparison to those of Wt observed here support the need to integrate the PQC mechanisms^{21,24} when generally establishing the main driving forces behind SGs-mediated sequestration of destabilized proteins (including disease-related mutations). In addition to SGs, unfolded and misfolded states also bind to chaperones,^{17,31,82,83} are targeted for degradation, or are accumulated in aggresomes and further cleared by autophagy,^{16,18,84,85} thus distributing the overall concentration of free unfolded species among these PQC centers.³¹ As such previous studies revealed, chaperones can act as suppressors of phase separation of unfolded states by binding to them preferentially in the diluted phase³¹ or can be

recruited inside SGs to prevent accumulation of misfolded proteins.¹⁸

Recent studies showed that many proteins involved in functional LLPS are expressed close to their solubility limits; thus, they are more prone to become less soluble with aging, leading to aggregation.⁸⁶ In this context, our current results built a foundation for achieving a global understanding concerning the involvement of unfolded states in LLPS, giving the intricate relation between dysfunctional unfolding, toxic aggregation, and aberrant liquid-to-solid phase transitions.^{24,87,88}

ASSOCIATED CONTENT

Supporting Information

The Supporting Information is available free of charge at <https://pubs.acs.org/doi/10.1021/jacs.1c09589>.

Description of materials and methods, visual and plot of aggregates of Wt and A4V mutants in HeLa^{FUS-mCh} cells; laser heating and FRET data; kinetic traces and amplitudes as a function of temperature; PCs of SOD1^{bar-Wt} and the various mutants inside SGs as a function of protein expression levels; correlation plot for SOD1_{bar} PCs; mobility of SOD1_{bar} inside SGs and cytosol after 120 minutes of HS; SDS PAGE gel for purified FUS-MBP and SOD1_{bar} constructs; DIC images of FUS droplets in the presence and absence of SOD1_{bar}; line-ROI intensity plots; images of SOD1_{bar} G4ID-enriched into or depleted from FUS-Wt droplets; change of the cross section of FUS droplets after HS at 43 °C with time; difference in ΔG_f° at 37 °C; PCs as a function of ΔG_f° ; LBMD simulation snapshots; interaction energies and contacts; fractions of protein surface areas occupied by the different residue types; mean number of contacts between different categories of residues; Tables S1 and S2 (including all the data points shown in the graphics) (PDF)

AUTHOR INFORMATION

Corresponding Authors

Stepan Timr – CNRS Laboratoire de Biochimie Théorique, Institut de Biologie Physico-Chimique, Université Paris Denis Diderot, Sorbonne Paris Cité, PSL Research University, Paris 75005, France; J. Heyrovský Institute of Physical Chemistry, Czech Academy of Sciences, Prague 8 182 23, Czech Republic; orcid.org/0000-0002-5824-4476; Email: stepan.timr@jh-inst.cas.cz

Fabio Sterpone – CNRS Laboratoire de Biochimie Théorique, Institut de Biologie Physico-Chimique, Université Paris Denis Diderot, Sorbonne Paris Cité, PSL Research University, Paris 75005, France; orcid.org/0000-0003-0894-8069; Email: fabio.sterpone@ibpc.fr

Simon Ebbinghaus – Institute of Physical and Theoretical Chemistry, TU Braunschweig, D-38106 Braunschweig, Germany; orcid.org/0000-0001-9309-1279; Email: s.ebbinghaus@tu-braunschweig.de

Authors

Nirnay Samanta – Institute of Physical and Theoretical Chemistry, TU Braunschweig, D-38106 Braunschweig, Germany; orcid.org/0000-0002-5746-6907

Sara S. Ribeiro – Institute of Physical and Theoretical Chemistry, TU Braunschweig, D-38106 Braunschweig, Germany; orcid.org/0000-0001-6033-8853

Mailin Becker – Institute of Physical and Theoretical Chemistry, TU Braunschweig, D-38106 Braunschweig, Germany

Emeline Laborie – CNRS Laboratoire de Biochimie Théorique, Institut de Biologie Physico-Chimique, Université Paris Denis Diderot, Sorbonne Paris Cité, PSL Research University, Paris 75005, France

Roland Pollak – Institute of Physical and Theoretical Chemistry, TU Braunschweig, D-38106 Braunschweig, Germany

Complete contact information is available at:
<https://pubs.acs.org/10.1021/jacs.1c09589>

Author Contributions

^{||}N.S. and S.S.R. contributed equally to this paper.

Funding

N.S., S.S.R. and SE acknowledge support by the German Research Foundation DFG-SPP 2191 “Molecular Mechanisms of Functional Phase Separation” (Project number 402723784). F.S., S.T., and E.L. acknowledge support from the “Initiative d’Excellence” program from the French State (Grant “DYNAMO”, ANR-11-LABX-0011–01). S.T. acknowledges funding from the European Union’s Horizon 2020 research and innovation program under the Marie Skłodowska-Curie grant agreement No 840395. Part of this work was carried out using HPC resources from GENCI and LBT.

Notes

The authors declare no competing financial interest.

ACKNOWLEDGMENTS

We thank Simon Alberti, Titus Franzmann, Danny Hatters, Jonas Ahlers and David Gnutz for helpful discussions and Simon Alberti and Dorothee Dormann for providing cells and FUS plasmids, respectively.

REFERENCES

- (1) Case, L. B.; Zhang, X.; Ditlev, J. A.; Rosen, M. K. Stoichiometry Controls Activity of Phase-Separated Clusters of Actin Signaling Proteins. *Science* **2019**, 363 (6431), 1093–1097.
- (2) Huang, W. Y. C.; Alvarez, S.; Kondo, Y.; Lee, Y. K.; Chung, J. K.; Lam, H. Y. M.; Biswas, K. H.; Kuriyan, J.; Groves, J. T. A Molecular Assembly Phase Transition and Kinetic Proofreading Modulate Ras Activation by SOS. *Science* **2019**, 363 (6431), 1098–1103.
- (3) Lu, Y.; Wu, T.; Gutman, O.; Lu, H.; Zhou, Q.; Henis, Y. I.; Luo, K. Phase Separation of TAZ Compartmentalizes the Transcription Machinery to Promote Gene Expression. *Nat. Cell Biol.* **2020**, 22 (4), 453–464.
- (4) Iserman, C.; Desroches Altamirano, C.; Jegers, C.; Friedrich, U.; Zarin, T.; Fritsch, A. W.; Mittasch, M.; Domingues, A.; Hersemann, L.; Jahnel, M.; et al. Condensation of Ded1p Promotes a Translational Switch from Housekeeping to Stress Protein Production. *Cell* **2020**, 181, 818.
- (5) Peeples, W.; Rosen, M. K. Mechanistic Dissection of Increased Enzymatic Rate in a Phase-Separated Compartment. *Nat. Chem. Biol.* **2021**, 17 (6), 693–702.
- (6) Riback, J. A.; Katanski, C. D.; Kear-Scott, J. L.; Pilipenko, E. V.; Rojek, A. E.; Sosnick, T. R.; Drummond, D. A. Stress-Triggered Phase Separation Is an Adaptive, Evolutionarily Tuned Response. *Cell* **2017**, 168 (6), 1028–1040.
- (7) Franzmann, T. M.; Jahnel, M.; Pozniakovskiy, A.; Mahamid, J.; Holehouse, A. S.; Nüske, E.; Richter, D.; Baumeister, W.; Grill, S. W.;

Pappu, R. V.; et al. Phase Separation of a Yeast Prion Protein Promotes Cellular Fitness. *Science* **2018**, 359 (6371), eaao5654.

(8) Petrovska, I.; Nüske, E.; Munder, M. C.; Kulasegaran, G.; Malinowska, L.; Kroschwald, S.; Richter, D.; Fahmy, K.; Gibson, K.; Verbavatz, J.-M.; Alberti, S. Filament Formation by Metabolic Enzymes Is a Specific Adaptation to an Advanced State of Cellular Starvation. *eLife* **2014**, 3, No. e02409.

(9) Munder, M. C.; Midtvedt, D.; Franzmann, T.; Nüske, E.; Otto, O.; Herbig, M.; Ulbricht, E.; Müller, P.; Taubenberger, A.; Maharana, S.; Malinowska, L.; Richter, D.; Guck, J.; Ziburdaev, V.; Alberti, S. A PH-Driven Transition of the Cytoplasm from a Fluid- to a Solid-like State Promotes Entry into Dormancy. *eLife* **2016**, 5, No. e09347.

(10) Wallace, E. W. J.; Kear-Scott, J. L.; Pilipenko, E. V.; Schwartz, M. H.; Laskowski, P. R.; Rojek, A. E.; Katanski, C. D.; Riback, J. A.; Dion, M. F.; Franks, A. M.; Airoidi, E. M.; Pan, T.; Budnik, B. A.; Drummond, D. A. Reversible, Specific, Active Aggregates of Endogenous Proteins Assemble upon Heat Stress. *Cell* **2015**, 162 (6), 1286–1298.

(11) Cabrera, M.; Boronat, S.; Marte, L.; Vega, M.; Pérez, P.; Ayté, J.; Hidalgo, E. Chaperone-Facilitated Aggregation of Thermo-Sensitive Proteins Shields Them from Degradation during Heat Stress. *Cell Rep.* **2020**, 30 (7), 2430–2443.

(12) Gallardo, P.; Salas-Pino, S.; Daga, R. R. Reversible Protein Aggregation as Cytoprotective Mechanism against Heat Stress. *Curr. Genet.* **2021**, 67, 849–855.

(13) Franzmann, T.; Alberti, S. Ubiquitin Protein Helps Cells to Recover from Stress. *Nature* **2021**, 597, 183–184.

(14) Zhao, L.; Vecchi, G.; Vendruscolo, M.; Körner, R.; Hayer-Hartl, M.; Hartl, F. U. The Hsp70 Chaperone System Stabilizes a Thermo-Sensitive Subproteome in *E. Coli*. *Cell Rep.* **2019**, 28 (5), 1335–1345.

(15) Vabulas, R. M.; Raychaudhuri, S.; Hayer-Hartl, M.; Hartl, F. U. Protein Folding in the Cytoplasm and the Heat Shock Response. *Cold Spring Harbor Perspect. Biol.* **2010**, 2 (12), a004390.

(16) Ganesan, S.; Rohde, G.; Eckermann, K.; Sroka, K.; Schaefer, M. K. E.; Dohm, C. P.; Kermer, P.; Haase, G.; Wouters, F.; Bähr, M.; Weishaupt, J. H. Mutant SOD1 Detoxification Mechanisms in Intact Single Cells. *Cell Death Differ.* **2008**, 15 (2), 312–321.

(17) Wood, R. J.; Ormsby, A. R.; Radwan, M.; Cox, D.; Sharma, A.; Vöpel, T.; Ebbinghaus, S.; Oliveberg, M.; Reid, G. E.; Dickson, A.; Hatters, D. M. A Biosensor-Based Framework to Measure Latent Proteostasis Capacity. *Nat. Commun.* **2018**, 9 (1), 287.

(18) Mateju, D.; Franzmann, T. M.; Patel, A.; Kopach, A.; Boczek, E. E.; Maharana, S.; Lee, H. O.; Carra, S.; Hyman, A. A.; Alberti, S. An Aberrant Phase Transition of Stress Granules Triggered by Misfolded Protein and Prevented by Chaperone Function. *EMBO J.* **2017**, 36 (12), 1669–1687.

(19) Boronat, S.; Cabrera, M.; Hidalgo, E. Spatial Sequestration of Misfolded Proteins as an Active Chaperone-Mediated Process during Heat Stress. *Curr. Genet.* **2021**, 67 (2), 237–243.

(20) Cherkasov, V.; Hofmann, S.; Druffel-Augustin, S.; Mogk, A.; Tyedmers, J.; Stoecklin, G.; Bukau, B. Coordination of Translational Control and Protein Homeostasis during Severe Heat Stress. *Curr. Biol.* **2013**, 23 (24), 2452–2462.

(21) Hipp, M. S.; Kasturi, P.; Hartl, F. U. The Proteostasis Network and Its Decline in Ageing. *Nat. Rev. Mol. Cell Biol.* **2019**, 20 (7), 421.

(22) Patel, A.; Lee, H. O.; Jawerth, L.; Maharana, S.; Jahnel, M.; Hein, M. Y.; Stoykov, S.; Mahamid, J.; Saha, S.; Franzmann, T. M.; Pozniakovskiy, A.; Poser, I.; Maghelli, N.; Royer, L. A.; Weigert, M.; Myers, E. W.; Grill, S.; Drechsel, D.; Hyman, A. A.; Alberti, S. A Liquid-to-Solid Phase Transition of the ALS Protein FUS Accelerated by Disease Mutation. *Cell* **2015**, 162 (5), 1066–1077.

(23) Marrone, L.; Drexler, H. C. A.; Wang, J.; Tripathi, P.; Distler, T.; Heisterkamp, P.; Anderson, E. N.; Kour, S.; Moraiti, A.; Maharana, S.; Bhatnagar, R.; Belgard, T. G.; Tripathy, V.; Kalmbach, N.; Hosseinzadeh, Z.; Crippa, V.; Abo-Rady, M.; Wegner, F.; Poletti, A.; Troost, D.; Aronica, E.; Busskamp, V.; Weis, J.; Pandey, U. B.; Hyman, A. A.; Alberti, S.; Goswami, A.; Sternecker, J. FUS Pathology in ALS Is Linked to Alterations in Multiple ALS-Associated Proteins

and Rescued by Drugs Stimulating Autophagy. *Acta Neuropathol.* **2019**, *138* (1), 67–84.

(24) Alberti, S.; Hyman, A. A. Biomolecular Condensates at the Nexus of Cellular Stress, Protein Aggregation Disease and Ageing. *Nat. Rev. Mol. Cell Biol.* **2021**, *22* (3), 196–213.

(25) Hofmann, S.; Kedersha, N.; Anderson, P.; Ivanov, P. Molecular Mechanisms of Stress Granule Assembly and Disassembly. *Biochim. Biophys. Acta, Mol. Cell Res.* **2021**, *1868* (1), 118876.

(26) Burke, K. A.; Janke, A. M.; Rhine, C. L.; Fawzi, N. L. Residue-by-Residue View of In Vitro FUS Granules That Bind the C-Terminal Domain of RNA Polymerase II. *Mol. Cell* **2015**, *60* (2), 231–241.

(27) Molliex, A.; Temirov, J.; Lee, J.; Coughlin, M.; Kanagaraj, A. P.; Kim, H. J.; Mittag, T.; Taylor, J. P. Phase Separation by Low Complexity Domains Promotes Stress Granule Assembly and Drives Pathological Fibrillization. *Cell* **2015**, *163* (1), 123–133.

(28) Guillén-Boixet, J.; Kopach, A.; Holehouse, A. S.; Wittmann, S.; Jahnel, M.; Schlüßler, R.; Kim, K.; Trussina, I. R. E. A.; Wang, J.; Mateju, D.; Poser, I.; Maharana, S.; Ruer-Gruß, M.; Richter, D.; Zhang, X.; Chang, Y.-T.; Guck, J.; Honigsmann, A.; Mahamid, J.; Hyman, A. A.; Pappu, R. V.; Alberti, S.; Franzmann, T. M. RNA-Induced Conformational Switching and Clustering of G3BP Drive Stress Granule Assembly by Condensation. *Cell* **2020**, *181* (2), 346–361.

(29) Conicella, A. E.; Zerze, G. H.; Mittal, J.; Fawzi, N. L. ALS Mutations Disrupt Phase Separation Mediated by α -Helical Structure in the TDP-43 Low-Complexity C-Terminal Domain. *Structure* **2016**, *24* (9), 1537–1549.

(30) Zhou, H.-X.; Nguemaha, V.; Mazarakos, K.; Qin, S. Why Do Disordered and Structured Proteins Behave Differently in Phase Separation? *Trends Biochem. Sci.* **2018**, *43* (7), 499–516.

(31) Ruff, K. M.; Choi, Y. H.; Cox, D.; Ormsby, A. R.; Myung, Y.; Ascher, D. B.; Radford, S. E.; Pappu, R. V.; Hatters, D. M. Sequence Grammar Underlying Unfolding and Phase Separation of Globular Proteins. *bioRxiv (Biophysics)*, August 20, 2021, 2021.08.20.457073. DOI: [10.1101/2021.08.20.457073](https://doi.org/10.1101/2021.08.20.457073) (accessed 2021–09–08).

(32) Ribeiro, S.; Ebbinghaus, S.; Marcos, J. C. Protein Folding and Quinary Interactions: Creating Cellular Organisation through Functional Disorder. *FEBS Lett.* **2018**, *592* (18), 3040–3053.

(33) Ribeiro, S. S.; Samanta, N.; Ebbinghaus, S.; Marcos, J. C. The Synergic Effect of Water and Biomolecules in Intracellular Phase Separation. *Nat. Rev. Chem.* **2019**, *3* (9), 552–561.

(34) Mathieu, C.; Pappu, R. V.; Taylor, J. P. Beyond Aggregation: Pathological Phase Transitions in Neurodegenerative Disease. *Science* **2020**, *370* (6512), 56–60.

(35) Jahn, T. R.; Radford, S. E. Folding versus Aggregation: Polypeptide Conformations on Competing Pathways. *Arch. Biochem. Biophys.* **2008**, *469* (1), 100–117.

(36) Grad, L. I.; Yerbury, J. J.; Turner, B. J.; Guest, W. C.; Pokrishevsky, E.; O'Neill, M. A.; Yanai, A.; Silverman, J. M.; Zeineddine, R.; Corcoran, L.; Kumita, J. R.; Luheshi, L. M.; Yousefi, M.; Coleman, B. M.; Hill, A. F.; Plotkin, S. S.; Mackenzie, I. R.; Cashman, N. R. Intercellular Propagated Misfolding of Wild-Type Cu/Zn Superoxide Dismutase Occurs via Exosome-Dependent and -Independent Mechanisms. *Proc. Natl. Acad. Sci. U. S. A.* **2014**, *111* (9), 3620–3625.

(37) Sen Mojumdar, S.; Scholl, Z. N.; Dee, D. R.; Rouleau, L.; Anand, U.; Garen, C.; Woodside, M. T. Partially Native Intermediates Mediate Misfolding of SOD1 in Single-Molecule Folding Trajectories. *Nat. Commun.* **2017**, *8* (1), 1881.

(38) Lang, L.; Zetterström, P.; Brännström, T.; Marklund, S. L.; Danielsson, J.; Oliveberg, M. SOD1 Aggregation in ALS Mice Shows Simplistic Test Tube Behavior. *Proc. Natl. Acad. Sci. U. S. A.* **2015**, *112* (32), 9878–9883.

(39) Gnutt, D.; Timr, S.; Ahlers, J.; König, B.; Manderfeld, E.; Heyden, M.; Sterpone, F.; Ebbinghaus, S. Stability Effect of Quinary Interactions Reversed by Single Point Mutations. *J. Am. Chem. Soc.* **2019**, *141* (11), 4660–4669.

(40) Wright, G. S. A.; Antonyuk, S. V.; Hasnain, S. S. The Biophysics of Superoxide Dismutase-1 and Amyotrophic Lateral Sclerosis. *Q. Rev. Biophys.* **2019**, *52*, e12.

(41) Gal, J.; Kuang, L.; Barnett, K. R.; Zhu, B. Z.; Shissler, S. C.; Korotkov, K. V.; Hayward, L. J.; Kasarskis, E. J.; Zhu, H. ALS Mutant SOD1 Interacts with G3BP1 and Affects Stress Granule Dynamics. *Acta Neuropathol.* **2016**, *132* (4), 563–576.

(42) Da Ros, M.; Deol, H. K.; Savard, A.; Guo, H.; Meiering, E. M.; Gibbins, D. Wild-Type and Mutant SOD1 Localizes to RNA-Rich Structures in Cells and Mice but Does Not Bind RNA. *J. Neurochem.* **2021**, *156* (4), 524–538.

(43) Danielsson, J.; Kurnik, M.; Lang, L.; Oliveberg, M. Cutting Off Functional Loops from Homodimeric Enzyme Superoxide Dismutase 1 (SOD1) Leaves Monomeric β -Barrels. *J. Biol. Chem.* **2011**, *286* (38), 33070–33083.

(44) Nordlund, A.; Leinartaitė, L.; Saraboji, K.; Aisenbrey, C.; Gröbner, G.; Zetterström, P.; Danielsson, J.; Logan, D. T.; Oliveberg, M. Functional Features Cause Misfolding of the ALS-Provoking Enzyme SOD1. *Proc. Natl. Acad. Sci. U. S. A.* **2009**, *106* (24), 9667–9672.

(45) Niwa, J.; Yamada, S.; Ishigaki, S.; Sone, J.; Takahashi, M.; Katsuno, M.; Tanaka, F.; Doyu, M.; Sobue, G. Disulfide Bond Mediates Aggregation, Toxicity, and Ubiquitylation of Familial Amyotrophic Lateral Sclerosis-Linked Mutant SOD1*. *J. Biol. Chem.* **2007**, *282* (38), 28087–28095.

(46) Ebbinghaus, S.; Dhar, A.; McDonald, J. D.; Gruebele, M. Protein Folding Stability and Dynamics Imaged in a Living Cell. *Nat. Methods* **2010**, *7* (4), 319–323.

(47) van Lente, J. J.; Claessens, M. M. A. E.; Lindhoud, S. Charge-Based Separation of Proteins Using Polyelectrolyte Complexes as Models for Membraneless Organelles. *Biomacromolecules* **2019**, *20* (10), 3696–3703.

(48) Raeburn, C. B.; Ormsby, A.; Moily, N. S.; Cox, D.; Ebbinghaus, S.; Dickson, A.; McColl, G.; Hatters, D. M. A Biosensor to Gauge Protein Homeostasis Resilience Differences in the Nucleus Compared to Cytosol of Mammalian Cells. *bioRxiv (Biochemistry)*, April 19, 2021, 2021.04.19.440383. DOI: [10.1101/2021.04.19.440383](https://doi.org/10.1101/2021.04.19.440383) (accessed 2021–09–08).

(49) Vassall, K. A.; Stubbs, H. R.; Primmer, H. A.; Tong, M. S.; Sullivan, S. M.; Sobering, R.; Srinivasan, S.; Briere, L.-A. K.; Dunn, S. D.; Colón, W.; Meiering, E. M. Decreased Stability and Increased Formation of Soluble Aggregates by Immature Superoxide Dismutase Do Not Account for Disease Severity in ALS. *Proc. Natl. Acad. Sci. U. S. A.* **2011**, *108* (6), 2210–2215.

(50) Wang, Q.; Johnson, J. L.; Agar, N. Y. R.; Agar, J. N. Protein Aggregation and Protein Instability Govern Familial Amyotrophic Lateral Sclerosis Patient Survival. *PLoS Biol.* **2008**, *6* (7), e170.

(51) Rauscher, S.; Pomès, R. The Liquid Structure of Elastin. *eLife* **2017**, *6*, No. e26526.

(52) Pettersen, E. F.; Goddard, T. D.; Huang, C. C.; Couch, G. S.; Greenblatt, D. M.; Meng, E. C.; Ferrin, T. E. UCSF Chimera—a Visualization System for Exploratory Research and Analysis. *J. Comput. Chem.* **2004**, *25* (13), 1605–1612.

(53) Hofweber, M.; Hutten, S.; Bourgeois, B.; Spreitzer, E.; Niedner-Boblentz, A.; Schifferer, M.; Ruepp, M.-D.; Simons, M.; Niessing, D.; Madl, T.; Dormann, D. Phase Separation of FUS Is Suppressed by Its Nuclear Import Receptor and Arginine Methylation. *Cell* **2018**, *173* (3), 706–719.

(54) Alexander, E. J.; Ghanbari Niaki, A.; Zhang, T.; Sarkar, J.; Liu, Y.; Nirujogi, R. S.; Pandey, A.; Myong, S.; Wang, J. Ubiquitin 2 Modulates ALS/FTD-Linked FUS–RNA Complex Dynamics and Stress Granule Formation. *Proc. Natl. Acad. Sci. U. S. A.* **2018**, *115* (49), E11485–E11494.

(55) Ahlers, J.; Adams, E. M.; Bader, V.; Pezzotti, S.; Winkhofer, K. F.; Tatzelt, J.; Havenith, M. The Key Role of Solvent in Condensation: Mapping Water in Liquid-Liquid Phase-Separated FUS. *Biophys. J.* **2021**, *120*, 1266.

- (56) Li, X.; Romero, P.; Rani, M.; Dunker, A. K.; Obradovic, Z. Predicting Protein Disorder for N-, C-, and Internal Regions. *Genome Inform. Workshop Genome Inform.* **1999**, *10*, 30–40.
- (57) Boeynaems, S.; Holehouse, A. S.; Weinhardt, V.; Kovacs, D.; Van Lindt, J.; Larabell, C.; Van Den Bosch, L.; Das, R.; Tompa, P. S.; Pappu, R. V.; Gitler, A. D. Spontaneous Driving Forces Give Rise to Protein–RNA Condensates with Coexisting Phases and Complex Material Properties. *Proc. Natl. Acad. Sci. U. S. A.* **2019**, *116*, 7889–7898.
- (58) Kaur, T.; Raju, M.; Alshareedah, I.; Davis, R. B.; Potoyan, D. A.; Banerjee, P. R. Sequence-Encoded and Composition-Dependent Protein–RNA Interactions Control Multiphasic Condensate Morphologies. *Nat. Commun.* **2021**, *12* (1), 872.
- (59) Dignon, G. L.; Zheng, W.; Kim, Y. C.; Mittal, J. Temperature-Controlled Liquid–Liquid Phase Separation of Disordered Proteins. *ACS Cent. Sci.* **2019**, *5* (5), 821–830.
- (60) Zwicker, D.; Seyboldt, R.; Weber, C. A.; Hyman, A. A.; Jülicher, F. Growth and Division of Active Droplets Provides a Model for Protocells. *Nat. Phys.* **2017**, *13* (4), 408–413.
- (61) Wang, J.; Choi, J.-M.; Holehouse, A. S.; Lee, H. O.; Zhang, X.; Jahnel, M.; Maharana, S.; Lemaitre, R.; Pozniakovskiy, A.; Drechsel, D.; Poser, I.; Pappu, R. V.; Alberti, S.; Hyman, A. A. A Molecular Grammar Governing the Driving Forces for Phase Separation of Prion-like RNA Binding Proteins. *Cell* **2018**, *174* (3), 688–699.
- (62) Lu, Y.; Lim, L.; Song, J. RRM Domain of ALS/FTD-Causing FUS Characteristic of Irreversible Unfolding Spontaneously Self-Assembles into Amyloid Fibrils. *Sci. Rep.* **2017**, *7* (1), 1–14.
- (63) Li, S.; Yoshizawa, T.; Yamazaki, R.; Fujiwara, A.; Kameda, T.; Kitahara, R. Pressure and Temperature Phase Diagram for Liquid–Liquid Phase Separation of the RNA-Binding Protein Fused in Sarcoma. *J. Phys. Chem. B* **2021**, *125* (25), 6821–6829.
- (64) Gnutt, D.; Brylski, O.; Edengeiser, E.; Havenith, M.; Ebbinghaus, S. Imperfect Crowding Adaptation of Mammalian Cells towards Osmotic Stress and Its Modulation by Osmolytes. *Mol. Biosyst.* **2017**, *13* (11), 2218–2221.
- (65) Gnutt, D.; Sistemich, L.; Ebbinghaus, S. Protein Folding Modulation in Cells Subject to Differentiation and Stress. *Front. Mol. Biosci.* **2019**, *6*, 38.
- (66) Senske, M.; Törk, L.; Born, B.; Havenith, M.; Herrmann, C.; Ebbinghaus, S. Protein Stabilization by Macromolecular Crowding through Enthalpy Rather than Entropy. *J. Am. Chem. Soc.* **2014**, *136* (25), 9036–9041.
- (67) Smith, A. E.; Zhou, L. Z.; Gorenssek, A. H.; Senske, M.; Pielak, G. J. In-Cell Thermodynamics and a New Role for Protein Surfaces. *Proc. Natl. Acad. Sci. U. S. A.* **2016**, *113* (7), 1725–1730.
- (68) Monteith, W. B.; Cohen, R. D.; Smith, A. E.; Guzman-Cisneros, E.; Pielak, G. J. Quinary Structure Modulates Protein Stability in Cells. *Proc. Natl. Acad. Sci. U. S. A.* **2015**, *112* (6), 1739–1742.
- (69) Cohen, R. D.; Pielak, G. J. Quinary Interactions with an Unfolded State Ensemble: Quinary Interactions & Unfolded State Ensemble. *Protein Sci.* **2017**, *26* (9), 1698–1703.
- (70) Samanta, N.; Mahanta, D. D.; Hazra, S.; Kumar, G. S.; Mitra, R. K. Short Chain Polyethylene Glycols Unusually Assist Thermal Unfolding of Human Serum Albumin. *Biochimie* **2014**, *104*, 81–89.
- (71) Sörensen, T.; Leeb, S.; Danielsson, J.; Oliveberg, M. Polyanions Cause Protein Destabilization Similar to That in Live Cells. *Biochemistry* **2021**, *60* (10), 735–746.
- (72) Kaur, T.; Alshareedah, I.; Wang, W.; Ngo, J.; Moosa, M. M.; Banerjee, P. R. Molecular Crowding Tunes Material States of Ribonucleoprotein Condensates. *Biomolecules* **2019**, *9* (2), 71.
- (73) Park, S.; Barnes, R.; Lin, Y.; Jeon, B.; Najafi, S.; Delaney, K. T.; Fredrickson, G. H.; Shea, J.-E.; Hwang, D. S.; Han, S. Dehydration Entropy Drives Liquid–Liquid Phase Separation by Molecular Crowding. *Commun. Chem.* **2020**, *3* (1), 1–12.
- (74) Nguemaha, V.; Zhou, H.-X. Liquid–Liquid Phase Separation of Patchy Particles Illuminates Diverse Effects of Regulatory Components on Protein Droplet Formation. *Sci. Rep.* **2018**, *8* (1), 6728.
- (75) Protter, D. S. W.; Rao, B. S.; Van Treeck, B.; Lin, Y.; Mizoue, L.; Rosen, M. K.; Parker, R. Intrinsically Disordered Regions Can Contribute Promiscuous Interactions to RNP Granule Assembly. *Cell Rep.* **2018**, *22* (6), 1401–1412.
- (76) Danielsson, J.; Mu, X.; Lang, L.; Wang, H.; Binolfi, A.; Theillet, F.-X.; Bekei, B.; Logan, D. T.; Selenko, P.; Wennerström, H.; Oliveberg, M. Thermodynamics of Protein Destabilization in Live Cells. *Proc. Natl. Acad. Sci. U. S. A.* **2015**, *112* (40), 12402–12407.
- (77) Ghosh, A.; Mazarakos, K.; Zhou, H.-X. Three Archetypical Classes of Macromolecular Regulators of Protein Liquid–Liquid Phase Separation. *Proc. Natl. Acad. Sci. U. S. A.* **2019**, *116* (39), 19474–19483.
- (78) André, A. A. M.; Spruijt, E. Liquid–Liquid Phase Separation in Crowded Environments. *Int. J. Mol. Sci.* **2020**, *21* (16), 5908.
- (79) Banani, S. F.; Rice, A. M.; Peeples, W. B.; Lin, Y.; Jain, S.; Parker, R.; Rosen, M. K. Compositional Control of Phase-Separated Cellular Bodies. *Cell* **2016**, *166* (3), 651–663.
- (80) Sterpone, F.; Melchionna, S.; Tuffery, P.; Pasquali, S.; Mousseau, N.; Cragnolini, T.; Chebaro, Y.; St-Pierre, J.-F.; Kalimeri, M.; Barducci, A.; Laurin, Y.; Tek, A.; Baaden, M.; Nguyen, P. H.; Derreumaux, P. The OPEP Protein Model: From Single Molecules, Amyloid Formation, Crowding and Hydrodynamics to DNA/RNA Systems. *Chem. Soc. Rev.* **2014**, *43* (13), 4871–4893.
- (81) Stirnemann, F.; Derreumaux, P.; Melchionna, S. Protein Simulations in Fluids: Coupling the OPEP Coarse-Grained Force Field with Hydrodynamics. *J. Chem. Theory Comput.* **2015**, *11* (4), 1843–1853.
- (82) Claes, F.; Rudyak, S.; Laird, A. S.; Louros, N.; Beerten, J.; Debulpaep, M.; Michiels, E.; van der Kant, R.; Van Durme, J.; De Baets, G.; Houben, B.; Ramakers, M.; Yuan, K.; Gwee, S. S. L.; Hernandez, S.; Broersen, K.; Oliveberg, M.; Moahamed, B.; Kirstein, J.; Robberecht, W.; Rousseau, F.; Schymkowitz, J. Exposure of a Cryptic Hsp70 Binding Site Determines the Cytotoxicity of the ALS-Associated SOD1-Mutant A4V. *Protein Eng., Des. Sel.* **2019**, *32* (10), 443–457.
- (83) Imamoglu, R.; Balchin, D.; Hayer-Hartl, M.; Hartl, F. U. Bacterial Hsp70 Resolves Misfolded States and Accelerates Productive Folding of a Multi-Domain Protein. *Nat. Commun.* **2020**, *11* (1), 1–13.
- (84) Gal, J.; Ström, A.-L.; Kilty, R.; Zhang, F.; Zhu, H. P62 Accumulates and Enhances Aggregate Formation in Model Systems of Familial Amyotrophic Lateral Sclerosis*. *J. Biol. Chem.* **2007**, *282* (15), 11068–11077.
- (85) Ciechanover, A.; Kwon, Y. T. Degradation of Misfolded Proteins in Neurodegenerative Diseases: Therapeutic Targets and Strategies. *Exp. Mol. Med.* **2015**, *47* (3), e147–e147.
- (86) Vecchi, G.; Sormanni, P.; Mannini, B.; Vandelli, A.; Tartaglia, G. G.; Dobson, C. M.; Hartl, F. U.; Vendruscolo, M. Proteome-Wide Observation of the Phenomenon of Life on the Edge of Solubility. *Proc. Natl. Acad. Sci. U. S. A.* **2020**, *117* (2), 1015–1020.
- (87) Dobson, C. M. Principles of Protein Folding, Misfolding and Aggregation. *Semin. Cell Dev. Biol.* **2004**, *15* (1), 3–16.
- (88) Zbinden, A.; Pérez-Berlanga, M.; De Rossi, P.; Polymenidou, M. Phase Separation and Neurodegenerative Diseases: A Disturbance in the Force. *Dev. Cell* **2020**, *55* (1), 45–68.